Received: 15 January 2021 | Revised: 24 June 2022 | Accepted: 27 June 2022

DOI: 10.1002/ppp.2160

RESEARCH ARTICLE

WILEY

Influence of ecosystem and disturbance on near-surface permafrost distribution, Whatì, Northwest Territories, Canada

Seamus V. Daly[1] | Philip P. Bonnaventure[1] | Will Kochtitzky[2,3]

[1]Bonnaventure Lab for Permafrost Science, Department of Geography and Environment, University of Lethbridge, Lethbridge, AB, Canada

[2]Department of Geography, Environment and Geomatics, University of Ottawa, Ottawa, ON, Canada

[3]Climate Change Institute, University of Maine, Orono, ME, USA

Correspondence
Seamus V. Daly, Bonnaventure Lab for Permafrost Science, Department of Geography and Environment, University of Lethbridge, Lethbridge, AB, Canada, T1K 3M4.
Email: seamus.daly@uleth.ca

Funding information
Climate Change Preparedness in the North Grant; Polar Geospatial Center; National Science Foundation Graduate Research Fellowship, Grant/Award Number: DGE-1144205; University of Lethbridge; Climate Change Preparedness

Abstract

For remote communities in the discontinuous permafrost zone, access to permafrost distribution maps for hazard assessment is limited and more general products are often inadequate for use in local-scale planning. In this study we apply established analytical methods to illustrate a time- and cost-efficient method for conducting community-scale permafrost mapping in the community of Whatì, Northwest Territories, Canada. We ran a binary logistic regression (BLR) using a combination of field data, digital surface model-derived variables, and remotely sensed products. Independent variables included vegetation, topographic position index, and elevation bands. The dependent variable was sourced from 139 physical checks of near-surface permafrost presence/absence sampled across the variable boreal–wetland environment. Vegetation is the strongest predictor of near-surface permafrost in the regression. The regression predicts that 50.0% (minimum confidence: 36%) of the vegetated area is underlain by near-surface permafrost with a spatial accuracy of 72.8%. Analysis of data recorded across various burnt and not-burnt environments indicated that recent burn scenarios have significantly influenced the distribution of near-surface permafrost in the community. A spatial burn analysis predicted up to an 18.3% reduction in near-surface permafrost coverage, in a maximum burn scenario without factoring in the influence of climate change. The study highlights the potential that in an ecosystem with virtually homogeneous air temperature, ecosystem structure and disturbance history drive short-term changes in permafrost distribution and evolution. Thus, at the community level these factors should be considered as seriously as changes to air temperature as climate changes.

KEYWORDS
boreal, empirical statistical, forest fire, logistic regression, permafrost

1 | INTRODUCTION

Communities in permafrost regions face uncertainties and challenges as climate warms and permafrost thaws. Many northern communities are becoming increasingly concerned with the adverse environmental and community impacts of thawing permafrost. Changes in hydrological regimes,[1,2] landscape instability, and hazards associated with thermokarst[3,4] are straining the relationship between northern communities and valuable ecosystem services,[5,6] such as quality of and access to country foods.[7,8] In addition to the impacts on traditional ways of life, permafrost thaw poses problems for both existing and future infrastructure including buildings, roads, and pipelines.[9–11] These issues are exacerbated by climate change[12] and natural disturbances common in the boreal forest environment, especially the presence of fire, which is presently occurring at a shorter recurrence interval over a longer season.[13,14]

Mapping the distribution of permafrost in the discontinuous permafrost zone of southern Northwest Territories (NT), Canada, is challenging. Although the terrain lacks major topographic relief, the landscape is heterogeneous with complex interactions between the boreal ecological community and prominent wetlands.[15] For some communities in the southern reaches of permafrost zones, changes are not only occurring with respect to climate but also with respect to the dynamics and structure of the built human communities themselves.[16] As a result, these communities are concerned with the distribution of permafrost, permafrost-related hazards, and infrastructure uncertainty.[17] As communities change and grow, there is a need for simple methods of permafrost detection and modeling to provide community stakeholders with the necessary information to make informed decisions on future development. Local-scale permafrost and hazard mapping is a relatively recent but popular field of study in permafrost sciences.[18–20] However, these studies require specific field data and high-resolution remote sensing products, meaning that a specific scientific study must take place to acquire this. In locations where these studies have not taken place, the scale and the representation of permafrost (e.g., continuity classes, temperature at the top of permafrost [TTOP]) in existing products can be an issue at the community level.[21] Many existing permafrost products use national-level maps derived from ground surface temperatures and broad classifications of substrate materials[22] or remote sensing data,[23] which cannot take into account local-scale variations that impact permafrost distribution and community uses of the land.

In many northern communities, recent changes in development and road connectivity are increasing interactions between people and permafrost. The objective of this study is to model the spatial distribution of permafrost in and around one such community to inform continued development. This study demonstrates a rapid and cost-effective method for mapping near-surface permafrost to inform development and future infrastructure. Climate data obtained from weather stations established in the study area in 2019 indicate that mean annual air temperature does not vary significantly across the study area (annually ≈ 0.1–0.3) (P. P. Bonnaventure, unpublished data). Despite this, the distribution of near-surface permafrost varies greatly, suggesting that the cause of such variability is ecosystem structure rather than air temperature. Near-surface permafrost is defined as permafrost existing in a state where the active layer freezes to the top of permafrost each winter and no talik exists between permafrost and the lowest depth of freeze back. Studies in the general area indicate that late-season active layer depth is less than 2 m,[24,25] so our use of near surface refers to permafrost within the first 2 m of the ground surface. Additionally, the community faces the constant possibility of fire (most recently occurring in 2014). The impact of fire on permafrost degradation has been well documented[26–29] and in this study we examine the impact of fire-induced landscape change on permafrost distribution using data collected from burnt and not-burnt sites. Ultimately the study illustrates that ecosystem structure and disturbance are impactful drivers of permafrost distribution and evolution in these landscapes, especially in the short term. As such, these influences should be considered as seriously as threats to the ecosystem service provided by permafrost as air temperature warming due to climate change.

1.1 | Study area

The study area is defined by the 60.0-km^2 municipal boundary of Whatì, NT (Figure 1). The community has a population of 470 people (2016) and is currently fly-in only during the summer but is connected to a seasonal road network during the winter months (Jan. 28 to Apr. 15).[30] In 2022, construction of a road connecting the community to the all-season road network is planned to be completed. This road is expected to increase the population and demand for infrastructure and services, yet a permafrost distribution map is not currently available for this area to inform development.

The study area is divided into a northern and a southern section by a ridge running east to west. The built community of Whatì (elevation of 247 m asl) is situated in the far west of the study area against the shores of Lac La Martre. The study area has a relief of 44 m, ranging from 238 to 282 m asl.

Whatì is classified as subarctic, with cool summers and year-round precipitation according to the Köppen-Geiger climate index (Dfc).[31] The closest long-term weather station is in Yellowknife, NT, 164 km to the southeast with a mean annual air temperature (MAAT) of −4.3°C and an annual average precipitation of 288.6 mm over the 1981–2010 climatic period. Only five months have a mean daily average above 0°C.[32]

Whatì falls into the extensive discontinuous permafrost zone according to the permafrost map of Canada,[22] indicating that 50–90% of the ground is underlain by permafrost. Ground ice content is categorized as low (considered to be less than 10% ice by volume of visible ice), in the upper 10–20 m.[22] The main species of vegetation found throughout the study area are spruce trees (*Picea*), deciduous trees such as aspen (*Populus*) and willow (*Salix*), Labrador tea (*Rhododendron*), buffaloberry (*Shepherdia*), fireweed (*Epilobium*), bearberry (*Arctostaphylos*), and mosses and lichens including peat moss (*Sphagnum*), reindeer lichen (*Cladonia*) and feathermoss (*Ptilium*) (Figure 2). The vegetation of the study area is mainly dependent on the local hydrology (drainage, water table, soil moisture) and is heterogeneous over short horizontal distances.

Summer 2014 was a record forest fire season. Roughly 84% of the study area was affected by the fires, with patches of unaffected vegetation. The fire stopped short of the built community due to anthropogenic and natural firebreaks.

2 | METHODS

2.1 | Cryotic assessment sites

We recorded data at 139 cryotic assessment sites (hereafter CASs) during the field season that took place over a 21-day period in August 2019 (Figure 1). CAS locations were sampled in the field across a

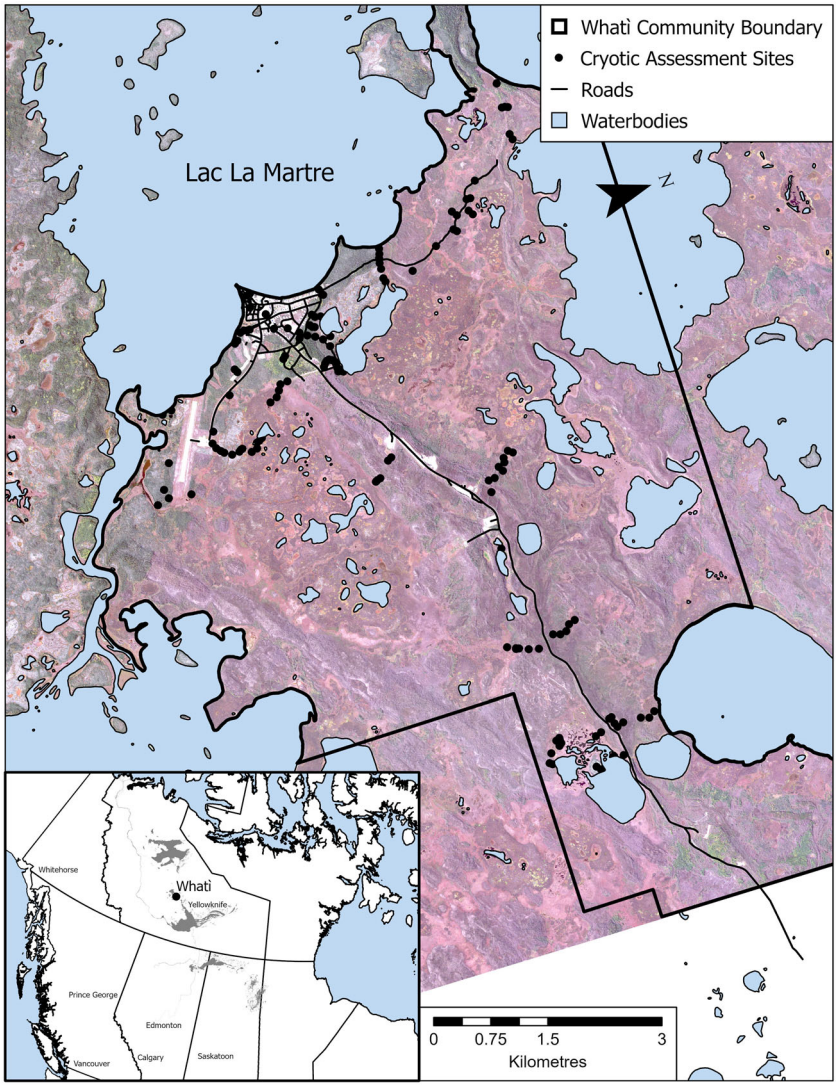

FIGURE 1 Study area extent. The extent of the built community as well as nondeveloped areas within the study area is indicated with the inclusion of the current road network and can be deduced from the base image included in the map. The base image shows both the heterogeneity of the environment and the effects of recent forest fires (2014). Black dots represent the 139 cryotic assessment sites recorded in August 2019. Inset map: location of the study area at a national scale; important bodies of water are included for reference (imagery © [2017] DigitalGlobe, Inc.) [Colour figure can be viewed at wileyonlinelibrary.com]

range of vegetation types, landcover classifications, and topographic relief.[19] Capturing the variation across vegetation types present in the study area was a key aspect of the field season as landcover is typically the main control on permafrost distribution in lowland boreal environments.[28,33]

To efficiently record CASs in the field, transects were created that passed through as many vegetation classes as possible with CASs recorded approximately every 150 m or where vegetation or terrain sharply changed.[19] The distribution of CASs is limited by access as the environment is difficult to traverse. While the CASs were recorded away from the influence of infrastructure (roads, off-road trails), they are clustered around these areas due to accessibility.

2.2 | Cryotic assessment site observations

Site observations at each CAS included thermal profiles[34] and major vegetation types.[35–37] We noted the ground cover characteristics, specifically the presence or absence of moss and lichen (*Sphagnum*, *Cladonia*, and *Ptilium*)[37] recorded as a binary variable (e.g., present or absent) and additional observations including site surroundings such as wetland, peat plateau, gravel features,[37] and areas affected by recent wildfires.[28,29] We recorded geographic position using a handheld GPS (Garmin GPSMAP 64x Series) using waypoint averaging (accuracy of 1–4 m).

CASs were sampled to determine presence or absence of near-surface permafrost.[34,38] Upon arriving at the location of a CAS, a soil probe (1.6 cm × 10.2 cm Extendible Tile Probe Complete) or portable hammer-drill (DeWalt Flexvolt 60 V MAX 4.0 cm Cordless SDS MAX, DCH481X2) was used to make a pilot hole with a target depth of 1.5 m.[24,33] Due to the substrate encountered in the study area, the soil probe was typically sufficient and most often used. When using the hammer drill holes were capped and left for a day prior to recording the thermal profile to minimize any thermal disturbances caused by the drill. Reaching a depth of 1.5 m was not always possible due to coarse substrate or the presence of near-surface permafrost above 1.5 m. This target depth was chosen as previous studies indicate that active layer thicknesses in the discontinuous permafrost region of the

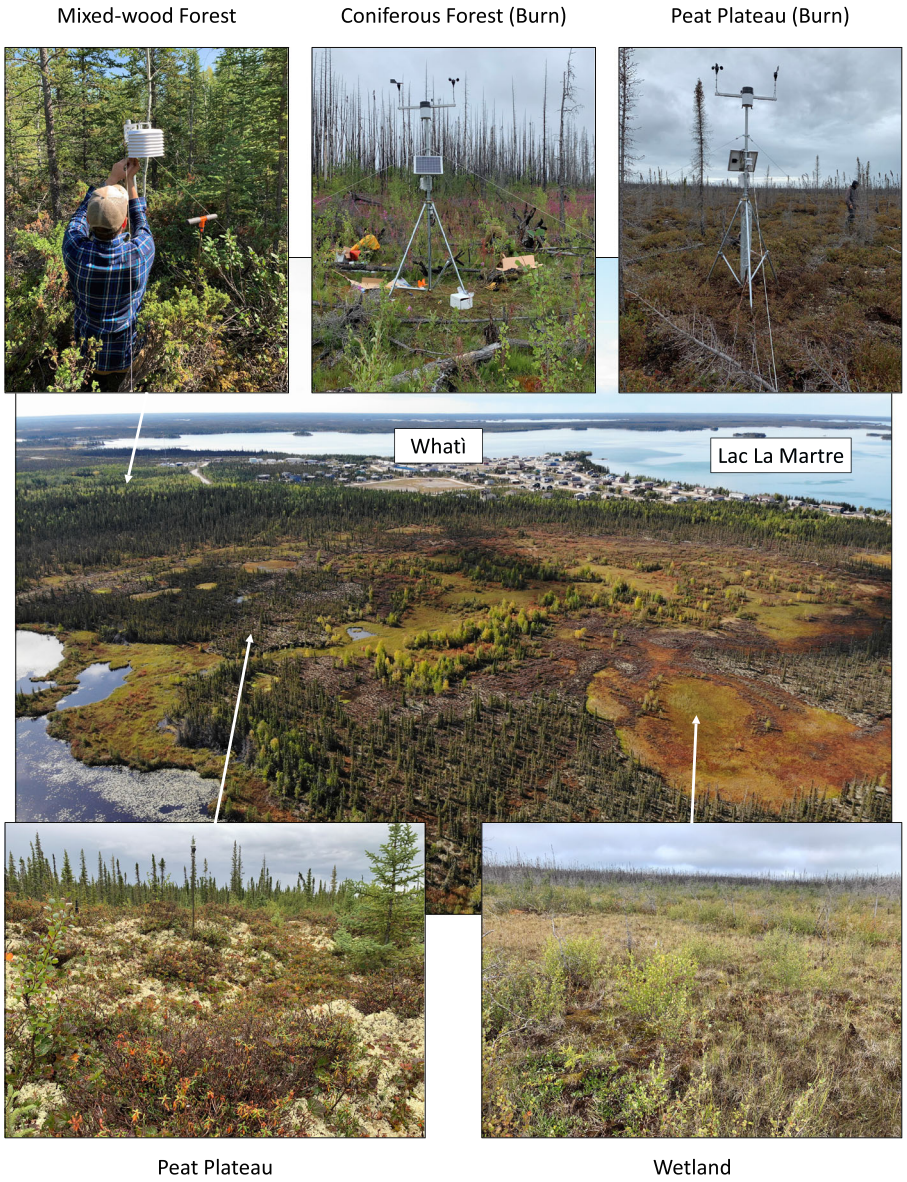

FIGURE 2 Common vegetation classes found throughout Whatì, NT. Five of the most common vegetation classes used in the study, mixed-wood forest, coniferous forest (burnt), peat plateau (burnt), peat plateau, and wetlands, are pictured. A less focused photo of the study area is provided, demonstrating the heterogenous environment in which the study was performed providing context to how these vegetation classes fit into the environment. Examples of burned environment throughout the study area are not pictured in the larger image [Colour figure can be viewed at wileyonlinelibrary.com]

NT boreal forest rarely exceed 1.5 m, although they can extend to 2.0 m in less common conditions.[24,25] The utilized methods do not account for taliks or post-burn active layer thickening that cause the frost table to exist below a depth of 2 m and thus can only detect near-surface permafrost. Our deepest CAS was 189 cm.

Once we created the pilot hole, we inserted a temperature probe into the hole and recorded a thermal profile (hole depths ranged from 30 to 189 cm). The temperature probe consisted of a modified carbon fiber avalanche probe with four thermistor cables (E348-TMC6-HD, accuracy: < ±0.2°C, resolution: < ±0.03°C). Three thermistor cables ran through the probe, each exiting the probe at a different depth. The depth spacing was at 0, 25, and 50 cm from the maximum depth[13] (bottom of probe) with one additional thermistor used to measure the ground surface temperature. Once the thermal probe was successfully inserted into the pilot hole all thermistor cables were plugged into a HOBO 4-Channel Analog Data Logger (UX120-006 M, accuracy: ±0.15°C, resolution: 0.002°C). The amount of time to reach equilibrium (5–12 min) varied depending on the temperature, moisture content, and substrate. Once all four channels were changing at a rate <0.01°C/min, we recorded the values and depths.[13,38,39] The amount of probe extending out of the ground was measured to determine the depth of the thermal probe.

2.3 | Analytical methods

The statistical relationship between environmental characteristics and manual checks of near-surface permafrost presence/absence was determined through the use of a binary logistic regression model performed in the statistical software SPSS[40] as well as ArcGIS Pro.[41] Three inputs, vegetation observations, topographic positioning index (TPI),[42] and elevation, are identified as being independent variables whereas ground temperature (presence or absence of permafrost) is the dependent variable. TPI is an algorithm (Equation 1)[43] that can be

applied across digital elevation models; it compares cells with neighboring cells in order to determine relative elevation. Positive values mean the cell is higher than its neighbors (hummock) and negative mean it is lower (hollow), which is useful for locating topographic depressions. Model input data were derived from CAS observations as well as optical imagery acquired from GeoEye on September 17, 2017 (Imagery © [2017] DigitalGlobe, Inc.). In this analysis probability refers to the likelihood that permafrost occurs at a given location as determined from the data and modeling.

$$tpi < scalefactor > = int((dem - focalmean(dem, annulus, irad, orad)) + .5) \quad (1)$$

Scalefactor = outer radius in map units
Irad = inner radius of annulus in cells
Orad = outer radius of annulus in cells

2.4 | Field data processing

The vegetation observations (plant species, ground cover) recorded at each CAS were synthesized into different vegetation classes based on vegetation species occurrence.[19] Coniferous forests, mixed-wood forests, and peat plateaus were split into burnt and not-burnt classes. Preliminary modeling was conducted with vegetation being broken into separate burnt and not-burnt classes. Vegetation classes where preliminary modeling showed that the presence or absence of near-surface permafrost varied depending on burn status were broken into burnt and not-burnt classes.

Each CAS that did not reach a depth of 1.5 m[24,33] or that indicated the presence of permafrost prior to 1.5 m ($n = 31$) was examined by plotting thermal gradient profiles in Excel.[34] Here the slope of the line was examined to determine if ground temperature would cross a threshold of 0.5°C by a depth of 1.5 m.[38,44] CASs were categorized as permafrost present if 0°C was crossed between a depth of 1.5 and 2 m.[13,38]

2.5 | Geospatial data processing

Independent variables used in the regression are elevation, TPI, and vegetation type. To quantify elevation and TPI we used a 2-m elevation model derived from GeoEye optical imagery taken on September 17, 2017 (Imagery © [2017] DigitalGlobe, Inc.). The surface model was produced by the Polar Geospatial Center at the University of Minnesota using the surface extraction with TIN-based search and space minimization (SETSM) algorithm.[45]

To confirm that the elevation model provided by the Polar Geospatial Center accurately represented the terrain and not a canopy height, we compared the elevation model to the only available ICESat-2 summer observations from August 10, 2019. We found a median difference of 24 cm among the 113 points that were common between ICESat-2 and the ArcticDEM strip. Five of our points had a difference of 3–10 m, but these were all in a small lake, indicating that ICESat-2 is seeing the bathymetry while our elevation model is seeing the surface of the lake. The difference of only 24 cm between the elevation model and ICESat-2, which penetrates vegetation coverage, gives us confidence that the elevation model is accurately providing the ground surface height in the study area.

In this study the elevation variable was used as a proxy for mineral-rich (gravel as well as larger stones) topographic features (Table 1). This assessment was made as a result of extensive field observations and local knowledge. A surficial geology map was not available at a comparable scale, so elevation breaks in the digital surface model were used to delineate these features. As the presence of well-drained gravel/till is typically associated with the absence of permafrost in discontinuous permafrost zones, it was important to be able to capture this spatially.[46,47]

Standing water, which accumulates in low TPI areas, reduces the likelihood of permafrost if it remains year-round.[33,48] Additionally, topographic depressions can capture drifting snow in winter, which prevents winter cooling of permafrost. Thus, areas with a deep snowpack are typically associated with higher ground or permafrost temperatures.[49,50]

To include TPI and elevation in the binary logistic regression, individual raster surfaces were created for TPI and elevation. The extract by points tool in ArcGIS Pro was then used to create a table that relates TPI and elevation to the CASs.

We used our vegetation field observations to inform a supervised classification to derive a spatially complete vegetation map in ENVI.[51] The supervised classification used the maximum-likelihood algorithm and was performed on an image stack made up of R, G, B, and NIR bands from the above-mentioned GeoEye image and a normalized difference vegetation index layer.[37,52] We smoothed the vegetation classification with a kernel size of 3 by 3 pixels and aggregate minimum size of 9 pixels to reduce the noise in the classification. The post-classification confusion matrix calculated in ENVI showed that the vegetation classification surface had an accuracy of 91%.

2.6 | Binary logistic regression

In SPSS Statistics[40] a random sampling regime was used on the processed data from the field, including vegetation, TPI, elevation, and near-surface permafrost presence (0 or 1) for each of the 139 CASs. The regime generated ten randomly sampled cross-validation pairs of testing (33%) and training data (67%). The full dataset was run in SPSS[40] through the BLRM tool. Backwards stepwise regression was used to evaluate each of the input variables. Vegetation, elevation, and TPI were deemed to be significant to the regression. BLRM generated coefficients for each variable as well as an intercept to determine the relative importance of each factor. The coefficients are represented by B_i and the intercept is represented by *int* in Equation 2[37]:

TABLE 1 Model input variables, including classes, descriptions, and coefficients (β) obtained through permafrost probability modeling. The number of cryotic assessment sites within each class is shown as *n*

Variables	Class	Description	*n*	Coverage (%)	β
Vegetation classification	Coniferous Forest (CC)	Black spruce and tamarack tree stands w/, organic mat. layer including: moss, lichen, Labrador tea, cinquefoil	19	8.3	90.8
	Coniferous Forest (Burnt) (CCB)	Same as *Coniferous Forest* with grass of *Parnassus*, sedges, and horsetails. Visible evidence of recent burn (2014)	14	9.2	50.3
	Low-shrub, Clearing (LSC)	Low-density paper birch, willow. Rose, horsetail, fireweed and grass	12	0.5	50.3
	Low-Shrub, Organic Mat. (LSOM)	Coniferous Forest adjacent, similar organic mat., low-density to no tree cover. Juniper, willow, spruce, Labrador tea, moss, lichen, cinquefoil	9	12.7	54.2
	Mixed-Wood Forest (MW)	Aspen, birch, willow, spruce, alder w/ thin organic mat. layer. Rose, buffalo berry, bear berry, occasional thin layer of moss and lichen	17	2.9	52.8
	Mixed-Wood Forest (Burnt) (MWB)	Same as *Mixed-Wood Forest* w/ fireweed. Visible evidence of recent burn (2014)	12	18.0	50.2
	Peat Plateau (PP)	Visible plateau or hummocky terrain. Cloudberry, bog rosemary, white lichen, moss, Labrador tea, spruce tree stands	16	3.2	73.9
	Peat Plateau (Burnt)	Same as *Peat Plateau* with visible evidence of burn (2014)	26	8.7	86.1
	Wetland (WL)	Wet moss layer, grass, bog birch, fireweed, sundew, wax mertle, willow, cinquefoil, bog rosemary. High water table. Minimal resistance to soil probe	14	36.6	50.9
Elevation[a]	1	≤ 246.8 m asl	13	23.3	50.0
	2	≤ 250.5 m asl	54	37.8	13.7
	3	≤ 255.3 m asl	52	24.4	16.4
	4	≤ 261.9 m asl	16	9.8	13.5
	5	≤ 282.7 m asl	4	4.6	0.0
Topographic Positioning Index (TPI)	1	≤−0.8	11	14.2	−5.2
	2	≤ 0.0	76	33.9	13.1
	3	≤ 1.1	48	44.2	15.0
	4	≤ 8.9	4	7.7	0.0
Constant					−81.2

[a]Elevation in this instance is being used as a proxy for surficial geology as major topography in the study area is dependent on surficial geology and our data suggested that surficial geology has an effect on the presence of permafrost.

$$P = \frac{1}{1 - e^{-\left(int + \sum_1^n B_i\right)}} \quad (2)$$

2.7 | Regression cross validation

Different iterations of the regression (10 random samplings of training data) were run in SPSS.[40] Of the 10 cross-validation pairs only one would be used to generate the final near-surface permafrost probability surface.[37] To determine which pair yielded the best results, four measures were observed: Nagelkerke R-square (range of results: 0.81–0.88), Hosmer and Lemshow significance test (range of results: 0.52–1.00), the accuracy of the training data (referred to as percentage correct) (range of results: 88.2–94.6%), and the accuracy of the testing data (referred to as agreement) (range of results: 80.4–89.1%) (Table 2). We calculated the "percentage correct" using the BLRM tool in SPSS[40] and measured the accuracy of the BLRM compared to the training data (Table 3). We calculated agreement in Excel, which represents the accuracy of the testing subsample when we apply the regression coefficients generated by the BLRM (Table 3). Table 3 provides a breakdown of the regression accuracy of the training and testing data for the testing pair that performed best when comparing the statistical measures detailed below.

TABLE 2 Results of each binary logistic regression model run in SPSS using each cross-validation pair. The highest values for each category are highlighted in light grey and in bold. VO refers to a model run using the random sampling pair for run 7 but only using vegetation as a model input

Run no.	Nagelkerke R^2	H&L sig. test	Percentage correct	Agreement	Average value	Average accuracy
1	0.81	0.89	88.2	**89.1**	87.0	88.7
2	0.88	0.95	92.9	80.4	89.1	86.7
3	0.83	0.99	90.3	82.6	88.8	86.5
4	0.85	0.99	92.5	84.8	90.4	88.7
5	0.85	0.99	90.3	80.4	88.8	85.4
6	**0.88**	0.99	93.5	80.4	90.4	87.0
7	0.86	**1.00**	91.4	87.0	**91.0**	**89.2**
8	0.86	0.52	92.5	82.6	78.3	87.6
9	0.82	0.52	91.4	84.8	77.6	88.1
10	0.88	0.99	**94.6**	80.4	90.7	87.5
VO	0.78	1.00	89.2	84.8	87.9	87.0

TABLE 3 Accuracy of the training and testing data for run 7 shown in Table 1. The "training data" confusion matrix is pulled from the results of the regression. The "testing data" confusion matrix is created by using the regression created using the training data to calculate the probability of the "testing data." A confusion matrix was then created. More details with regard to this process can be found in the "Regression cross validation" section

		Predicted					
		Training data (% correct)			Testing data (agreement)		
		Permafrost			Permafrost		
Observed		Absent	Present	Correct (%)	Absent	Present	Correct (%)
Permafrost	Absent	36	4[b]	90.0	15	1[b]	93.8
	Present	4[a]	49	92.5	5[a]	25	83.3
	Overall (%)			91.4			88.5

[a]False positive.
[b]False negative.

The four measures were consistent across all 10 of the pairs. The only measure with a significant range was the Hosmer and Lemshow significance test (range: 0.52–1.00), which was 0.52 for cross-validation pairs eight and nine. The testing pair selected for use in the study is number seven in Table 2. This run has the highest average value of 91.0% (the average of all four measures with r^2 and significance test adjusted to be out of 100) and the highest average accuracy (89.2%, average of percentage correct and agreement; Table 2).

2.8 | Near-surface permafrost probability model

The near-surface permafrost probability model was created by reclassifying the raster surfaces of the independent variables (vegetation, elevation, TPI) to represent the coefficients obtained from the BLRM in SPSS.[40] These were then inserted into Equation 2 in the ArcGIS Pro[41] raster calculator to create the final near-surface permafrost probability surface (Figure 3). A flowchart depiciting the steps taken to generate this model can be found in the supplement (Supplement Figure S1). This yielded a 2-m resolution raster that displays the percentage probability of near-surface permafrost being present in any given pixel.

3 | RESULTS

3.1 | Field results

Of the 139 CASs created during the 2019 field season, we recorded 83 locations with near-surface permafrost (either initially in the field or in post-processing) and 56 without. Vegetation observations were recorded and synthesized into nine unique classes. The classes are burnt coniferous forest, coniferous forest, low-shrub clearing, low-shrub organic matter mixed-wood forest, burnt mixed-wood forest, peat plateau, burnt peat plateau, and wetland. One-time measurements of active layer thickness (ALT) were recorded in the field at each CAS (August 2019). Analysis of these data showed that ALT in the study area ranges from 40 to 180 cm. Figure 4 shows ALT for each vegetation class.

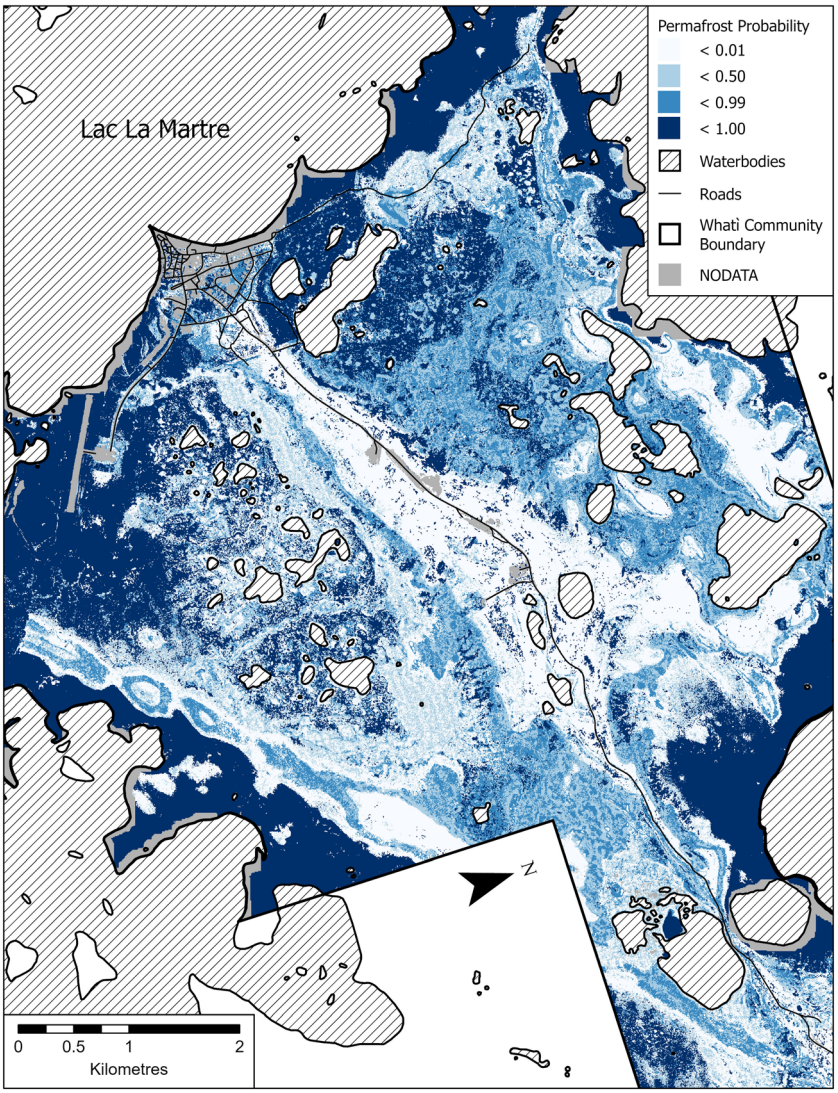

FIGURE 3 The permafrost probability surface generated for the community of Whatì. The probability surface was generated at a 2-m resolution by using the results of a binary logistic regression model that was populated using data recorded in the field at 139 cryotic assessment sites. Roads and the community boundary are included to tie the probability surface to the study area. Areas not included in the regression model (built infrastructure) are represented as "NODATA." Four breaks are shown in the probability model, and two extremes (< 0.1 and < 1.00) which represent the two extremes of the probability model. The < 0.1 class represents cells with a near zero chance of containing permafrost and the < 1.00 class represents cells with a near zero chance of being permafrost-absent. The two remaining classes show the remaining data split at 50% chance of containing permafrost [Colour figure can be viewed at wileyonlinelibrary.com]

3.2 | Vegetation classification

Landcover percentages in the study area are shown in Figure 5. Vegetation covers 84.9% of the study area with the remaining 15.1% representing waterbodies and infrastructure (13.3 and 1.8% respectively). Wetlands make up 34.9% of the vegetation cover, burnt mixed-wood forest makes up 19.5%, and low-shrub, organic matter makes up 12.7%. Burnt coniferous, burnt peat plateau, and coniferous forests each cover 8.9, 9.6, and 8.7% respectively (Figure 5).

3.3 | Model output

Probability refers to the likelihood that permafrost occurs at a given location as determined from the data and modeling. The probability map shows the likely spatial distribution of near-surface permafrost within the community boundary of Whatì (Figure 3). It predicts that 50.0% of the study area is underlain by near-surface permafrost with 10% of the pixels having a probability of less than 1% and 36% having a probability of greater than 99%. Individual pixels in the study area must be assessed as either 0 or 100% probability although 1,000 pixels with identical probability values of 10% would indicate that near-surface permafrost is expected to be found in 100 pixels.[38] For example, the vegetation class low-shrub organic matter (LSOM) has a mean probability of 0.75, indicating that 75% of the cells classified as LSOM are expected to be underlain by near-surface permafrost, which equates to 1,086,467 pixels that have been classified as LSOM are expected to be underlain by permafrost. A table that includes all possible modelled probability values for each vegetation class can be found in the supplement (Supplement Table S1).

The distribution of near-surface permafrost in the study area is skewed towards the upper and lower extremes; 32% of the area falls between 1 and 25% and 10% falls between 75 and 99%. These results support the notion that ecosystem structure, and surface characteristics including hydrology are driving permafrost distribution rather than simply mean annual air temperature.[47] Middle values representing probability of 25–75% are predicted for only 12% of the pixels in the near-surface permafrost probability map.

Of the three variables used in the regression, we found the greatest correlation between vegetation and the probability surface. This is

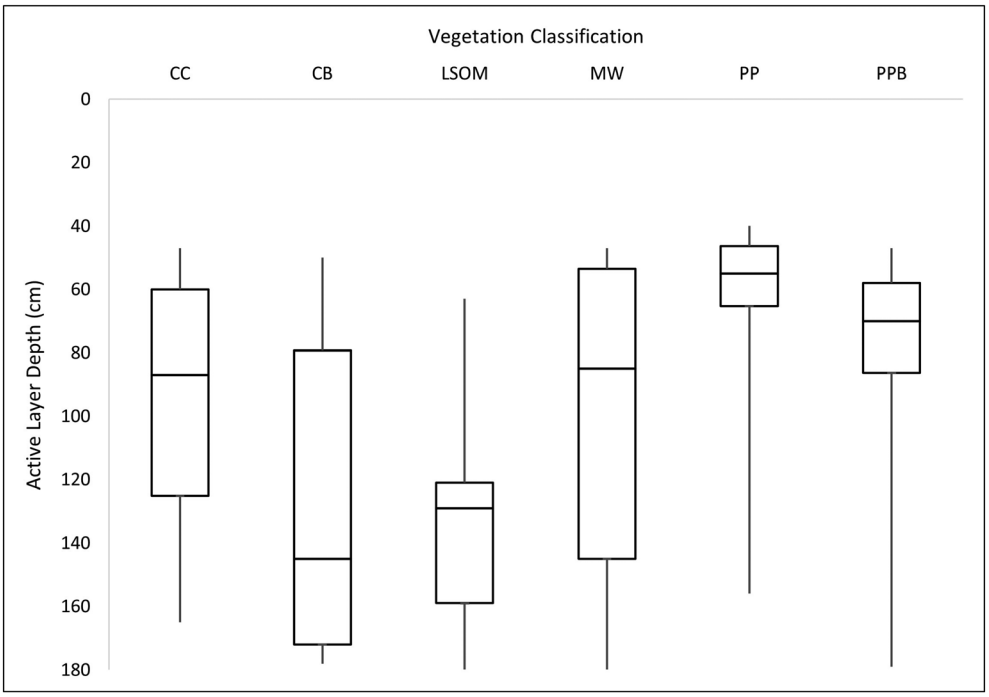

FIGURE 4 Box and whisker plots of the distribution of active layer thicknesses measured in the field (August 2019). Active layer thickness measurements are broken down into respective vegetation classes. Only cryotic assessment sites where permafrost was recorded as present are included in the graph. Vegetation classes such as low-shrub clearing, mixed-wood (burnt) and wetlands are not included due to a lack of sites where permafrost was recorded as being present. CC = coniferous forest, CB = coniferous forest (burnt), LSC = low-shrub, clearing, LSOM = low-shrub, organic matter, MW = mixed-wood forest, MWB = mixed-wood forest (burnt), PP = peat plateau, PPB = peat plateau (burnt), WL = wetland

evident as the magnitude of coefficients derived from the BLRM tool is far greater for vegetation (50.2–90.8) than for either elevation or TPI (−5.2 to 50.0; Table 1). Higher coefficients lead to higher near-surface permafrost probabilities as the intercept in this regression is −81.2. The vegetation classes that were correlated with high probability of near-surface permafrost presence were low-shrub organic matter (71.0% of pixels classified as permafrost present [>50%]), peat plateau (99.0%), burnt peat plateau (99.9%), and coniferous forest (100.0%). These four classes account for 32.9% of the total area of the probability map. The wetlands vegetation classification accounts for 36.6% of the probability map (Figure 6), and 32.9% of the wetland pixels were classified as having near-surface permafrost. Even though cells classified as wetland have a low near-surface permafrost probability, they cover such a large area that they contain 11.8% of the near-surface permafrost in the study area. The remaining classes, low-shrub clearing (30.9% of pixels classified as near-surface permafrost present [>50%]), mixed-wood burnt (26.1%), mixed-wood (36.8%) and coniferous forests burnt (34.0%), make up 30.5% of the probability map.

4 | DISCUSSION

4.1 | Interclass variability

Except for the peat plateau, burnt peat plateau, and coniferous forest classes, which have minimal interclass variability, the predicted probability values of all vegetation classes have some degree of interclass variability. This variability is caused by specific influences of the other two variables in the model (TPI and elevation). As mentioned in the previous section, the wetland class has the greatest coverage in the study area (36.6%) and this class accounts for 24.6% of the near-surface permafrost-absent cells in the study area and 11.8% of the permafrost-present cells. All possible combinations of variable in the model containing wetlands predicted probabilities lower than 50% except for elevation class 1 with any TPI class or elevation class 3 with TPI class 3 (Table 1). This is also true for vegetation classes with similar coefficients to the wetland class (CCB, LSC, MWB). This variability shows that while vegetation is the most important variable in the model, elevation and TPI act as important modifiers that can tip the balance of the predicted probability to one side of the 50% threshold.

4.2 | Model accuracy assessment

While the binary logistic regression has an accuracy of 91.4% (Table 3), this does not represent the accuracy of the probability model. To assess this, the generated probability surface (Figure 3) was compared to the assessment of near-surface permafrost presence in the CASs ($n = 139$). Agreement (%) was based on whether the probability model agreed with the assessment of presence/absence in the CASs. The agreement value is 72.8%. The disagreement (27.2%) could be caused by errors in data collection, but is probably due to errors in the

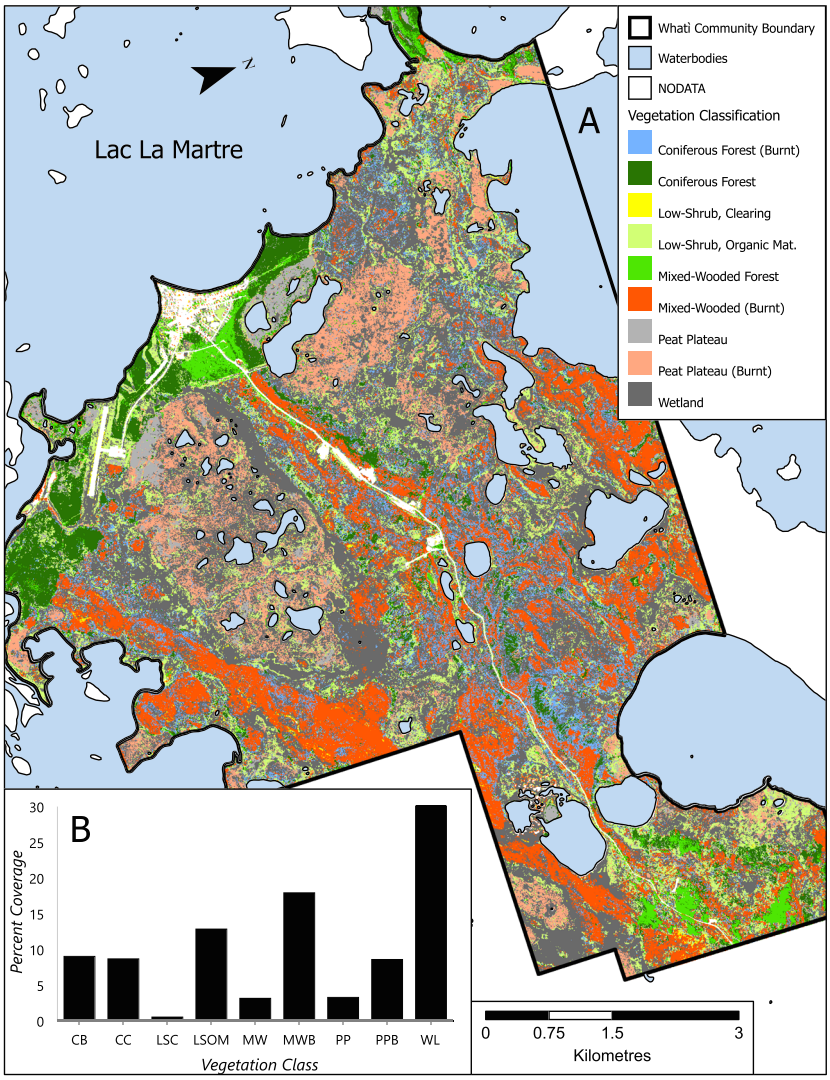

FIGURE 5 A: supervised vegetation classification created in ENVI using an image stack made up of R, G, B, and NIR bands from GeoEye optical imagery (imagery © [2017] DigitalGlobe, Inc.) and an NDVI surface derived from the same imagery. B: graph showing the percentage of area covered by each class in the vegetation classification surface. CC = coniferous forest, CB = coniferous forest (burnt), LSC = low-shrub, clearing, LSOM = low-shrub, organic matter (a class that represents a similar forest floor to coniferous forests, but without tree cover), MW = mixed-wood forest, MWB = mixed-wood forest (burnt), PP = peat plateau, PPB = peat plateau (burnt), WL = wetland [Colour figure can be viewed at wileyonlinelibrary.com]

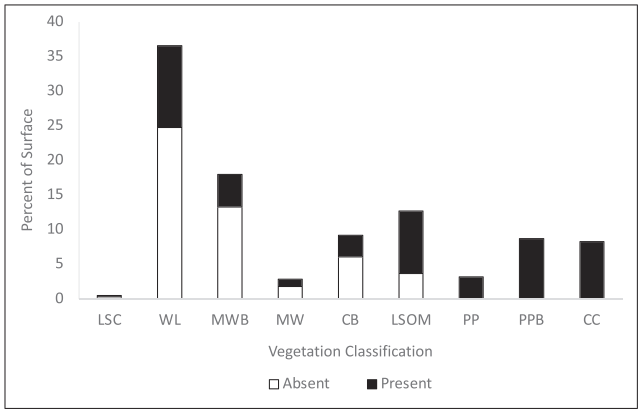

FIGURE 6 Graph representing cells classified as permafrost present and absent and their percentage contribution to the final probability surface for each vegetation class. CC = coniferous forest, CB = coniferous forest (burnt), LSC = low-shrub, clearing, LSOM = low-shrub, organic matter, MW = mixed-wood forest, MWB = mixed-wood forest (burnt), PP = peat plateau, PPB = peat plateau (burnt), WL = wetland

vegetation classification or possibly a control on permafrost presence that is not captured in the model. The model was verified using a related testing subset and not an independent verification dataset, and the sampling method used to select the sites where the testing and training subsets were recorded in the field was not entirely random, so the actual accuracy values may be lower than calculated in this study.[53]

4.3 | Burn analysis

In the last century, forest fires in the northern boreal forest have increased both in severity and in frequency.[14,54] As such, understanding how permafrost responds to fire disturbance is key to understanding the evolution of its spatial distribution. The modeled coefficients of three vegetation classes contained variations depending on whether recent burn was experienced (Table 1). Of these classes, coniferous forests (coefficients: not-burnt, 90.79; burnt, 50.29) represented the most substantial change in predicted permafrost probability when shifting from not-burnt to burnt, while mixed-wood

(coefficients: not-burnt, 52.75; burnt, 50.17) and peat plateau (coefficients: not burnt, 73.92; burnt, 86.05) only changed marginally.

To examine the potential impact of fire on permafrost distribution in the study area we tested two scenarios: (a) the entire landscape burns ($burn_{100}$) and (b) none of the landscape burns ($burn_0$). To create these surfaces, we changed all cells classified as burnt/not-burnt to either burnt ($burn_{100}$) or not-burnt ($burn_0$). Compared to the probability model, which shows an average near-surface permafrost probability of 50.0%, $burn_{100}$ results in a reduction in near-surface permafrost coverage of 6.2% to 43.8%. $Burn_0$ resulted in an increase in coverage of 12.1% to 62.1%. These scenarios illustrate the impact fire can have in determining the future near-surface permafrost distribution in Whatí and is independent of any applied climate change.

The effects of fire on permafrost vary greatly and are typically dependent on both antecedent conditions and burn severity.[28] The most important factors influencing post-fire permafrost stability are antecedent organic layer thickness, remaining organic layer thickness post-fire, post-fire soil moisture content, and the speed of vegetation succession and regrowth to pre-fire conditions.[33,55,56] Results from the probability model support this as peat plateau shows very little difference in the probability of near-surface permafrost regardless of its burnt status (Figure 7).

Peatlands are often more resilient to fire as they typically have a higher soil moisture content due to poorly drained fine-grained soils,[26,29,57] and there is also the possibility for near-surface permafrost to prevent drainage causing a high water table which also increases resiliency to deep burns.[58] This is apparent in a comparison of ALT between burnt peat-plateau (80.5 cm) and peat plateau (64.0 cm), which represents a difference of 16.5 cm (Figure 4). In areas of low burn severity, where moss and other surface organics remain, the effect of the burn may be less severe and moss could fully recover in two or three decades.[59] In burnt forests, the reduction in the tree canopy resulting in decreased snow interception is considered to be one of the greatest factors leading to the degradation of permafrost and thickening of the active layer.[60] This provides an explanation for why the greatest change (coefficients: not-burnt, 90.79; burnt, 50.29) due to burn is observed in coniferous forests where tree stands were burned, reducing interception to near zero, and organic ground cover was not as thick as in the peat plateaus.

4.4 | Ecosystem robustness to climate change

As the probability model does not involve climate inputs, we cannot project permafrost presence based on future climate scenarios, but they are still worth discussing in the context of this model as, along with forest fire activity, they will determine the future of permafrost in Whatí. In particular we want to understand whether the rate of ecosystem succession is fast enough to combat the speed of predicted warming. RCP4.5 and RCP8.5[61,62] projections were examined for the study area for the 2050 (2041–2060) and 2080 (2071–2100) forecasted climate normals derived from CMIP5.[63] With a historical MAAT of −5°C (1981–2010), RCP4.5 predicts an MAAT of −2.2°C (Δ +2.8) for 2050 and −1.4°C (Δ +3.6) for 2080.[61,62] RCP8.5 however, predicts an MAAT of −1.1°C (Δ +3.9) and 1.6°C (Δ +6.6) for 2050 and 2080 respectively.[61,62] Smith et al (2015) concluded that regrowth of a boreal environment after a burn would take 50 years and a predicted rise in MAAT of 3°C (MAAT of 1981–2010 climate normal for Smith et al's (2015) study area = −5.1°C) over that span was enough that permafrost in burnt environments would probably not return to pre-burn conditions until complete regrowth occurs. Looking at the 2050 projection for RCP4.5, the rise in temperature is +2.8°C for Whatí, just short of that 3°C threshold found by Smith et al (2015). However, RCP8.5 represents a rise of 3.6°C, well past the threshold. This indicates that in the 50 years from the 2014 burn in Whatì, MAAT is expected to increase by at least 2.8°C, which would probably prevent permafrost from returning to pre-burn conditions even after the local ecosystem has returned to pre-burn conditions.[60] This illustrates that both a combination of ecosystem structural changes and predicted air temperature warming must be considered in an examination of possible permafrost change in these environments.

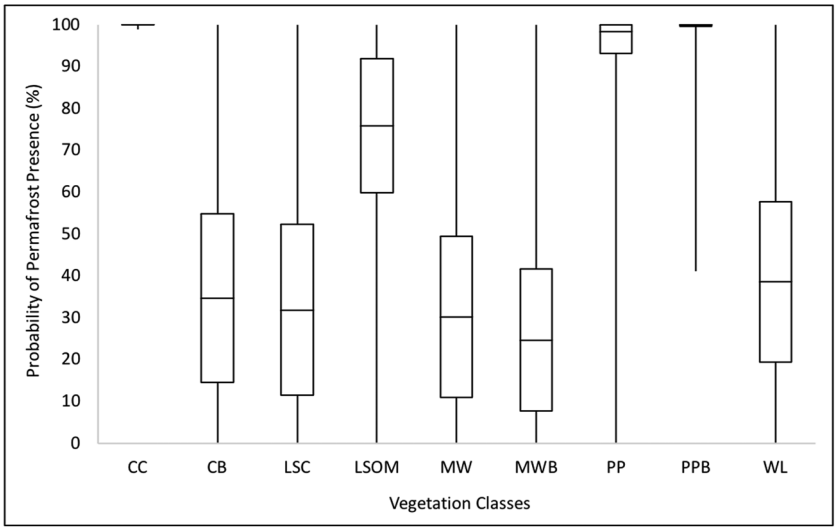

FIGURE 7 Box and whiskers plot representing the distribution (range, average, standard deviation) of permafrost probability generated by the model for each vegetation class. CC = coniferous forest, CB = coniferous forest (burnt), LSC = low-shrub, clearing, LSOM = low-shrub, organic matter, MW = mixed-wood forest, MWB = mixed-wood forest (burnt), PP = peat plateau, PPB = peat plateau (burnt), WL = wetland

4.5 | Uncertainty and improvements

There are a few ways our model could be improved with better observations. The number of CASs across all vegetation types is uneven and, in some situations, unrepresentative of the ground cover per cent of specific classes. This issue also impacts our elevation classes, specifically elevation class 1, which is underrepresented (13 of 139) in our sampling data but makes up 50% of our study area (Table 1). Further expansion of the CAS coverage would be useful as it would allow for larger amounts of training data and better landcover class representation, although this is challenging given the difficult access to the entire study area when the ground is not frozen.

The vegetation classification is another source of uncertainty. Incorporating better ground truth data and/or airborne observations (e.g., thermal imagery) would help improve the model.[64–66] Radar or lidar would also have helped as the structure of wetlands could vary significantly from other classes such as burnt coniferous forest.[67–69]

Weather stations in each landcover class are not available for the study area, and therefore temperature measurements are not incorporated into this model. This limits our ability to adjust the model for future climate scenarios. If these data were available, an approach utilizing these data such as a temperature at the top of permafrost would be prudent for modeling permafrost temperature in the area.[70]

5 | CONCLUSIONS

This study presents an effective way to quantify the distribution of permafrost around northern communities. The methodology is highly transferable, and the results of the model provide considerably more permafrost spatial information at higher resolutions than has previously been available from regional models. For the community of Whatì this is valuable as the Community Government expects the recently completed all-season road (opened to the public November 30, 2021) to increase population, land use, and development projects in the near future.

Using a binary logistic regression model derived from physical checks of permafrost presence/absence as the dependent variable, and vegetation, elevation, and TPI as independent variables, we created a permafrost probability surface for the community of Whatì, NT. According to the regression, 50.0% of the vegetated area is underlain by permafrost. This regression has a statistical accuracy of 91.4% and an agreement between spatial model values and ground-truth data of 72.8%.

Local ecology was key in modeling permafrost presence. Vegetation classes with undisturbed tree cover as well as thick organic soils and vegetated ground surfaces were strong indicators of permafrost presence. The classes include low-shrub organic matter, coniferous forest, peat-plateau and burnt peat-plateau. The opposite was the case for classes with near-surface mineral soils and more bare ground such as mixed-wood forest, burnt mixed-wood forest, and low-shrub, clearing.

The likelihood of near-surface permafrost varied across burnt/not-burnt pairs. The most significant occurrence of this is between coniferous forests and burnt coniferous forests. The burn changed coniferous forests from a class with a 100% prediction rate of near-surface permafrost to one with a 34% prediction rate. To examine ecosystem sensitivity to fire disturbance, we modeled two scenarios, a full burn across the landscape and no burn across the landscape. The full burn scenario resulted in a 6% reduction in overall near-surface permafrost coverage to 43.8% based on our model results. In the no burn scenario, near-surface permafrost coverage increased to 62.1%.

The results of this research illustrate that understanding the distribution and evolution of boreal wetland permafrost is highly complex. Boreal wetland environments are extremely heterogeneous with permafrost distribution having been shown to be highly sensitive to disturbance. This study highlights that disturbance itself in the short term can lead to punctuated and rapid permafrost changes. When disturbance is combined with predicted warming, permafrost becomes exceptionally vulnerable. As a result, it is prudent that future studies in similar regions consider both the impact of ecosystem structure and associated changes as seriously as a warming climate.

ACKNOWLEDGEMENTS

We thank the Community Government of Whatì for their driving role and continued support for the project and acknowledge the Tłı̨chǫ Traditional Territory on which this study took place. Funding for this project was provided by the Climate Change Preparedness in the North Program. We also thank the Natural Sciences and Engineering Research Council, the University of Lethbridge, and the Government of Northwest Territories, Geological Survey for funding contributions and research support. W.K. was supported by the National Science Foundation Graduate Research Fellowship under Grant No. DGE-1144205 and the Vanier Graduate Scholarship. WorldView imagery and DSMs were provided to W.K. by the Polar Geospatial Center under NSF-OPP awards 1043681, 1559691, and 1542736. We thank Kyle Bexte and Collin Simpson for field assistance, Madeleine Garibaldi for assistance with data, and Oliver K. Kienzle for assistance with editing.

DATA AVAILABILITY STATEMENT

The data that support the findings are owned by the Community Government of Whatì and managed by the University of Lethbridge. All data products from this work are available.

ORCID

Seamus V. Daly https://orcid.org/0000-0003-1809-7421

REFERENCES

1. Connon RF, Quinton WL, Craig JR, Hayashi M. Changing hydrologic connectivity due to permafrost thaw in the lower Liard River valley, NWT, Canada. *Hydrol Process*. 2014;28(14):4163-4178. doi:10.1002/hyp.10206
2. Quinton W, Hayashi M, Chasmer L. Permafrost-thaw-induced land-cover change in the Canadian subarctic: implications for water resources. *Hydrol Process*. 2011;25(1):152-158. doi:10.1002/hyp.7894

3. Nelson FE, Anisimov OA, Shiklomanov NI. Subsidence risk from thawing permafrost. *Nature*. 2001;410(6831):889-890. doi:10.1038/35073746
4. Nelson FE, Anisimov OA, Shiklomanov NI. Climate change and hazard zonation in the circum-Arctic permafrost regions. *Nat Hazards*. 2002;26(3):203-225. doi:10.1023/A:1015612918401
5. Gibson CM, Brinkman T, Cold H, Brown D, Turetsky M. Identifying increasing risks of hazards for northern land-users caused by permafrost thaw: integrating scientific and community-based research approaches. *Environ Res Lett*. 2021;16(6):064047. doi:10.1088/1748-9326/abfc79
6. Trochim E, Schuur E, Schaedel C, Kelly BP. Impacts of Permafrost on Infrastructure and Ecosystem Services. Paper presented at: AGU Fall Meeting Abstracts2017.
7. Calmels F, Laurent C, Brown R, Pivot F, Ireland M. How permafrost thaw may impact food security of Jean Marie River First Nation, NWT. In: *Paper presented at: 68th Canadian geotechnical conference and 7th Canadian permafrost conference*. Quebec City, Canada: GEOQuebec2015.
8. Spring A, Carter B, Blay-Palmer A. Climate change, community capitals, and food security: building a more sustainable food system in a northern Canadian boreal community. *Can Food Stud/La Revue Canadienne Des études Sur l'alimentation*. 2018;5(2):111-141. doi:10.15353/cfs-rcea.v5i2.199
9. Bommer C, Phillips M, Arenson LU. Practical recommendations for planning, constructing and maintaining infrastructure in mountain permafrost. *Permafr Periglac Process*. 2010;21(1):97-104. doi:10.1002/ppp.679
10. Doré G, Niu F, Brooks H. Adaptation methods for transportation infrastructure built on degrading permafrost. *Permafr Periglac Process*. 2016;27(4):352-364. doi:10.1002/ppp.1919
11. Hjort J, Karjalainen O, Aalto J, et al. Degrading permafrost puts Arctic infrastructure at risk by mid-century. *Nat Commun*. 2018;9(1):1-9. doi:10.1038/s41467-018-07557-4
12. Anisimov OA, Nelson FE. Permafrost zonation and climate change in the northern hemisphere: results from transient general circulation models. *Clim Change*. 1997;35(2):241-258. doi:10.1023/A:1005315409698
13. Holloway JE, Lewkowicz AG. Half a century of discontinuous permafrost persistence and degradation in western Canada. *Permafr Periglac Process*. 2020;31(1):85-96. doi:10.1002/ppp.2017
14. Wang X, Thompson DK, Marshall GA, Tymstra C, Carr R, Flannigan MD. Increasing frequency of extreme fire weather in Canada with climate change. *Clim Change*. 2015;130(4):573-586. doi:10.1007/s10584-015-1375-5
15. Jorgenson MT, Harden J, Kanevskiy M, et al. Reorganization of vegetation, hydrology and soil carbon after permafrost degradation across heterogeneous boreal landscapes. *Environ Res Lett*. 2013;8(3):035017. doi:10.1088/1748-9326/8/3/035017
16. Streletskiy D, Anisimov O, Vasiliev A. Chapter 10—Permafrost Degradation. In: Shroder JF, Haeberli W, Whiteman C, eds. *Snow and ice-related hazards, risks and disasters*:303-344. doi:10.1016/B978-0-12-394849-6.00010-X.
17. Ou C, LaRocque A, Leblon B, Zhang Y, Webster K, McLaughlin J. Modelling and mapping permafrost at high spatial resolution using Landsat and Radarsat-2 images in northern Ontario, Canada: part 2–regional mapping. *Int J Remote Sens*. 2016;37(12):2751-2779. doi:10.1080/01431161.2016.1151574
18. Flynn M, Ford JD, Labbé J, Schrott L, Tagalik S. Evaluating the effectiveness of hazard mapping as climate change adaptation for community planning in degrading permafrost terrain. *Sustain Sci*. 2019;14(4):1041-1056. doi:10.1007/s11625-018-0614-x
19. Whitley MA, Frost GV, Jorgenson MT, Macander MJ, Maio CV, Winder SG. Assessment of LiDAR and spectral techniques for high-resolution mapping of sporadic permafrost on the Yukon-Kuskokwim Delta, Alaska. *Remote Sens (Basel)*. 2018;10(2):258. doi:10.3390/rs10020258
20. Zhang Y. Spatio-temporal features of permafrost thaw projected from long-term high-resolution modeling for a region in the Hudson Bay lowlands in Canada. *J Geophys Res Earth*. 2013;118(2):542-552. doi:10.1002/jgrf.20045
21. Zhang Y, Wang X, Fraser R, et al. Modelling and mapping climate change impacts on permafrost at high spatial resolution for an Arctic region with complex terrain. *Cryosphere*. 2013;7(4):1121-1137. doi:10.5194/tc-7-1121-2013
22. Heginbottom J, Dubreuil M, Harker P. *Canada, permafrost. National Atlas of Canada. Natural resources Canada*. 5thed. MCR; 1995:4177.
23. Obu J, Westermann S, Bartsch A, et al. Northern hemisphere permafrost map based on TTOP modelling for 2000–2016 at 1 km2 scale. *Earth Sci Rev*. 2019;193:299-316. doi:10.1016/j.earscirev.2019.04.023
24. Nixon FM, Taylor AE. Regional active layer monitoring across the sporadic, discontinuous and continuous permafrost zones, Mackenzie Valley, northwestern Canada. Paper presented at: Proceedings of the Seventh International Conference on Permafrost 1998.
25. Wolfe SA. *Living with frozen ground: A field guide to permafrost in Yellowknife, Northwest Territories*. Vol. 64. Geological Survey of Canada; 1998.
26. Genet H, McGuire AD, Barrett K, et al. Modeling the effects of fire severity and climate warming on active layer thickness and soil carbon storage of black spruce forests across the landscape in interior Alaska. *Environ Res Lett*. 2013;8(4):045016. doi:10.1088/1748-9326/8/4/045016
27. Gibson CM, Chasmer LE, Thompson DK, Quinton WL, Flannigan MD, Olefeldt D. Wildfire as a major driver of recent permafrost thaw in boreal peatlands. *Nat Commun*. 2018;9(1):1-9. doi:10.1038/s41467-018-05457-1
28. Holloway JE, Lewkowicz AG, Douglas TA, et al. Impact of wildfire on permafrost landscapes: a review of recent advances and future prospects. *Permafr Periglac Process*. 2020;31(3):371-382. doi:10.1002/ppp.2048
29. Jafarov EE, Romanovsky VE, Genet H, McGuire AD, Marchenko SS. The effects of fire on the thermal stability of permafrost in lowland and upland black spruce forests of interior Alaska in a changing climate. *Environ Res Lett*. 2013;8(3):035030. doi:10.1088/1748-9326/8/3/035030
30. Government of the Northwest Territories DoI. Winter Roads Average Open/Close Dates. Department of Infrastructure https://wwwinfgovntca/en/services/highways-ferries-and-winter-roads/winter-roads-average-openclose-dates. Updated November 9, 2020. Accessed September 10, 2020.
31. Peel MC, Finlayson BL, McMahon TA. Updated world map of the Köppen-Geiger climate classification. 2007.
32. Canada Go. *Canadian climate Normals 1981–2010 station data*. Government of Canada, Environment and Natural Resources. https://climate.weather.gc.ca/climate_normals/results_1981_2010_e.html?stnID=1706&autofwd=1. Updated September 17, 2020. Accessed September 10, 2020.
33. Fisher JP, Estop-Aragonés C, Thierry A, et al. The influence of vegetation and soil characteristics on active-layer thickness of permafrost soils in boreal forest. *Glob Chang Biol*. 2016;9(22):3127-3140. doi:10.1111/gcb.13248
34. Bonnaventure PP, Lewkowicz AG. Mountain permafrost probability mapping using the BTS method in two climatically dissimilar locations, Northwest Canada. *Can J Earth Sci*. 2008;45(4):443-455. doi:10.1139/E08-013
35. Jorgenson MT. Hierarchical organization of ecosystems at multiple spatial scales on the Yukon-Kuskokwim Delta, Alaska, USA. *Arct Antarct Alp Res*. 2000;32(3):221-239. doi:10.1080/15230430.2000.12003360

36. Anderson JE, Douglas TA, Barbato RA, Saari S, Edwards JD, Jones RM. Linking vegetation cover and seasonal thaw depths in interior Alaska permafrost terrains using remote sensing. *Remote Sens Environ*. 2019;233:111363. doi:10.1016/j.rse.2019.111363
37. Panda SK, Prakash A, Solie DN, Romanovsky VE, Jorgenson MT. Remote sensing and field-based mapping of permafrost distribution along the Alaska highway corridor, interior Alaska. *Permafr Periglac Process*. 2010;21(3):271-281. doi:10.1002/ppp.686
38. Lewkowicz AG, Ednie M. Probability mapping of mountain permafrost using the BTS method, Wolf Creek, Yukon territory, Canada. *Permafr Periglac Process*. 2004;15(1):67-80. doi:10.1002/ppp.480
39. Bonnaventure PP, Lewkowicz AG, Kremer M, Sawada MC. A permafrost probability model for the southern Yukon and northern British Columbia, Canada. *Permafr Periglac Process*. 2012;23(1):52-68. doi:10.1002/ppp.1733
40. IBM SPSS Statistics for Windows. Version 26.0. IBM Corp. https://www.ibm.com/analytics/spss-statistics-software
41. ArcGIS Pro. Version 2.6.2. ESRI 2020. https://www.esri.com/en-us/arcgis/products/arcgis-pro/overview
42. Jenness J. *Topographic position index (tpi_jen. Avx) extension for ArcView 3. X, v. 1.3 a*. Jenness EnterprisesIn; 2006.
43. Weiss A. Topographic position and landforms analysis. Paper presented at: Poster presentation, ESRI user conference, San Diego, CA2001.
44. Bonnaventure PP, Lewkowicz AG. Permafrost probability modeling above and below treeline, Yukon, Canada. *Cold Reg Sci Technol*. 2012;79:92-106.
45. Noh M-J, Howat IM. The surface extraction from TIN based search-space minimization (SETSM) algorithm. *ISPRS J Photogramm Remote Sens*. 2017;129:55-76. doi:10.1016/j.isprsjprs.2017.04.019
46. Romanovsky V, Osterkamp T. Interannual variations of the thermal regime of the active layer and near-surface permafrost in northern Alaska. *Permafr Periglac Process*. 1995;6(4):313-335. doi:10.1002/ppp.3430060404
47. Shur Y, Jorgenson M. Patterns of permafrost formation and degradation in relation to climate and ecosystems. *Permafr Periglac Process*. 2007;18(1):7-19. doi:10.1002/ppp.582
48. Higgins KL, Garon-Labrecque MÈ. Fine-scale influences on thaw depth in a forested peat plateau landscape in the Northwest Territories, Canada: vegetation trumps microtopography. *Permafr Periglac Process*. 2018;29(1):60-70. doi:10.1002/ppp.1961
49. Bonnaventure PP, Lamoureux SF, Favaro EA. Over-Winter Channel bed temperature regimes generated by contrasting snow accumulation in a high Arctic River. *Permafr Periglac Process*. 2017;28(1):339-346. doi:10.1002/ppp.1902
50. Way RG, Lewkowicz AG. Environmental controls on ground temperature and permafrost in Labrador, Northeast Canada. *Permafr Periglac Process*. 2018;29(2):73-85. doi:10.1002/ppp.1972
51. ENVI. 5.5. L3 Harris Geospatial Solutions. 2008.
52. Tucker C, Sellers P. Satellite remote sensing of primary production. *Int J Remote Sens*. 1986;7(11):1395-1416. doi:10.1080/01431168608948944
53. Congalton RG, Green K. *Assessing the accuracy of remotely sensed data: Principles and practices*. CRC press; 2019.
54. Kasischke ES, Verbyla DL, Rupp TS, et al. Alaskas changing fire regime—implications for the vulnerability of its boreal forests. *Can J for Res*. 2010;40(7):1313-1324. doi:10.1139/X10-098
55. Jiang Y, Rocha AV, O'Donnell JA, et al. Contrasting soil thermal responses to fire in Alaskan tundra and boreal forest. *J Geophys Res Earth*. 2015;120(2):363-378. doi:10.1002/2014JF003180
56. Yi S, McGuire AD, Kasischke E, et al. A dynamic organic soil biogeochemical model for simulating the effects of wildfire on soil environmental conditions and carbon dynamics of black spruce forests. *J Geophys Res Biogeo*. 2010;115:G4. doi:10.1029/2010JG001302
57. Zhang Y, Wolfe SA, Morse PD, Olthof I, Fraser RH. Spatiotemporal impacts of wildfire and climate warming on permafrost across a subarctic region, Canada. *J Geophys Res Earth*. 2015;120(11):2338-2356. doi:10.1002/2015JF003679
58. Turetsky M, Donahue W, Benscoter B. Experimental drying intensifies burning and carbon losses in a northern peatland. *Nat Commun*. 2011;2(1):1-5. doi:10.1038/ncomms1523
59. Turetsky MR, Mack MC, Hollingsworth TN, Harden JW. The role of mosses in ecosystem succession and function in Alaskas boreal forest. *Can J for Res*. 2010;40(7):1237-1264. doi:10.1139/X10-072
60. Smith SL, Riseborough DW, Bonnaventure PP. Eighteen year record of forest fire effects on ground thermal regimes and permafrost in the Central Mackenzie Valley, NWT, Canada. *Permafr Periglac Process*. 2015;26(4):289-303. doi:10.1002/ppp.1849
61. AdaptWest Project. Gridded current and projected climate data for North America at 1 km resolution, interpolated using the *ClimateNA v5. 10* software (T. Wang et al., 2015). Available at adaptwest.databasin.org. 2015.
62. Wang T, Hamann A, Spittlehouse D, Carroll C. Locally downscaled and spatially customizable climate data for historical and future periods for North America. *PLoS ONE*. 2016;11(6):e0156720. doi:10.1371/journal.pone.0156720
63. Taylor KE, Stouffer RJ, Meehl GA. An overview of CMIP5 and the experiment design. *Bull Am Meteorol Soc*. 2012;93(4):485-498. doi:10.1175/BAMS-D-11-00094.1
64. Fuentes DA, Gamon JA, Hl Q, Sims DA, Roberts DA. Mapping Canadian boreal forest vegetation using pigment and water absorption features derived from the AVIRIS sensor. *J Geophys Res Atmos*. 2001;106(D24(D24):33565-33577. doi:10.1029/2001JD900110
65. Larsen PF, Phinney DA, Rubin F, Justice D. Classification of boreal macrotidal littoral zone habitats in the Gulf of Maine: comparison of IKONOS and CASI multispectral imagery. *Geocarto Int*. 2009;24(6):457-472. doi:10.1080/10106040802677029
66. Price JC. The contribution of thermal data in Landsat multispectral classification. *Photogramm Eng Remote Sens*. 1981;47(2):229-236.
67. Chasmer L, Hopkinson C, Veness T, Quinton W, Baltzer J. A decision-tree classification for low-lying complex land cover types within the zone of discontinuous permafrost. *Remote Sens Environ*. 2014;143:73-84. doi:10.1016/j.rse.2013.12.016
68. Korpela I, Koskinen M, Vasander H, Holopainen M, Minkkinen K. Airborne small-footprint discrete-return LiDAR data in the assessment of boreal mire surface patterns, vegetation, and habitats. *For Ecol Manage*. 2009;258(7):1549-1566. doi:10.1016/j.foreco.2009.07.007
69. Morsdorf F, Meier E, Kötz B, Itten KI, Dobbertin M, Allgöwer B. LIDAR-based geometric reconstruction of boreal type forest stands at single tree level for forest and wildland fire management. *Remote Sens Environ*. 2004;92(3):353-362. doi:10.1016/j.rse.2004.05.013
70. Riseborough D, Shiklomanov N, Etzelmüller B, Gruber S, Marchenko S. Recent advances in permafrost modelling. *Permafr Periglac Process*. 2008;19(2):137-156. doi:10.1002/ppp.615

SUPPORTING INFORMATION

Additional supporting information can be found online in the Supporting Information section at the end of this article.

How to cite this article: Daly SV, Bonnaventure PP, Kochtitzky W. Influence of ecosystem and disturbance on near-surface permafrost distribution, Whatì, Northwest Territories, Canada. *Permafrost and Periglac Process*. 2022; 1-14. doi:10.1002/ppp.2160